

ORIGINAL ARTICLE

# Grown, Printed, and Biologically Augmented: An Additively Manufactured Microfluidic Wearable, Functionally Templated for Synthetic Microbes

Christoph Bader,<sup>1,\*</sup> William G. Patrick,<sup>1,\*</sup> Dominik Kolb,<sup>1</sup> Stephanie G. Hays,<sup>2,3</sup> Steven Keating,<sup>1</sup>  
Sunanda Sharma,<sup>1</sup> Daniel Dikovsky,<sup>4</sup> Boris Belocon,<sup>4</sup> James C. Weaver,<sup>3</sup> Pamela A. Silver,<sup>2,3</sup> and Neri Oxman<sup>1</sup>

## Abstract

Despite significant advances in synthetic biology at industrial scales, digital fabrication challenges have, to date, precluded its implementation at the product scale. We present, *Mushtari*, a multimaterial 3D printed fluidic wearable designed to culture microbial communities. Thereby we introduce a computational design environment for additive manufacturing of geometrically complex and materially heterogeneous fluidic channels. We demonstrate how controlled variation of geometrical and optical properties at high spatial resolution can be achieved through a combination of computational growth modeling and multimaterial bitmap printing. Furthermore, we present the implementation, characterization, and evaluation of support methods for creating product-scale fluidics. Finally, we explore the cytotoxicity of 3D printed materials in culture studies with the model microorganisms, *Escherichia coli* and *Bacillus subtilis*. The results point toward design possibilities that lie at the intersection of computational design, additive manufacturing, and synthetic biology, with the ultimate goal of imparting biological functionality to 3D printed products.

## Introduction

### Vision

HOW CAN WE design relationships between the most primitive and the most sophisticated life forms? Can we design wearables embedded with synthetic microorganisms that enhance and augment biological functionality? We explored these questions through the creation of *Mushtari* (Fig. 1), a 3D printed wearable that comprised 58 meters of internal fluid channels. The wearable concept piece was designed to function as a “microbial factory” that uses genetically modified microbes to make useful products for the wearer.

Optimally, *Mushtari* could enable and inform a symbiotic relationship between two microorganisms: photosynthetic autotrophs, such as microalgae or cyanobacteria, and compatible heterotrophs, such as *Escherichia coli* or *Bacillus subtilis*. The photosynthetic microbes could convert sunlight into nutrients for the heterotrophs, which could in turn produce compounds for specific applications. This form of microbial symbiosis, a phenomenon commonly found in nature,<sup>1</sup> builds upon the in-

herent symbiosis present between the wearer and the microbes *within* the wearable. Based on the demonstrated biocompatibility for microbes shown in cytotoxicity tests of the 3D printed materials used in this study, we ultimately envision a fully functional photosynthetic prototype that contains engineered heterotrophs such that the wearer would be able to trigger microbial production of specific compounds of interest, including scents,<sup>2</sup> pigments,<sup>3</sup> and fuels.<sup>4</sup>

While 3D printing has been previously demonstrated as a viable means for the production of bespoke wearable-scale products,<sup>5</sup> this technology has not previously been used to print a wearable with an inner fluidic network. Until recently, additive manufacturing has been utilized to produce microfluidic devices,<sup>6</sup> but only in a single material and/or typically at a small scale—usually below feature sizes of 10 cm—when compared to the scale of a typical wearable. *Mushtari* is the first of its kind fluidic device with channels as thin as 1 mm in diameter. It was digitally fabricated at a wearable scale and examines the material ecology<sup>7</sup> within a 3D printed wearable that incorporates functional microbial communities.

<sup>1</sup>MIT Media Laboratory, School of Architecture and Planning, Massachusetts Institute of Technology, Cambridge, Massachusetts.

<sup>2</sup>Department of Systems Biology, Harvard Medical School, Boston, Massachusetts.

<sup>3</sup>Wyss Institute for Biologically Inspired Engineering, Harvard University, Cambridge, Massachusetts.

<sup>4</sup>Stratasys, LTD., Rehovot, Israel.

\*Cofirst authors.



FIG. 1. Side view of *Mushtari*. The 3D printed wearable combines a continuous internal network of biocompatible fluidic channels with variable optical transparency through the use of bitmap-based multimaterial additive manufacturing. *Mushtari* was produced in collaboration with Stratasys Ltd. on an Objet 500 Connex 3 Multimaterial 3D printer. Photo: Yoram Reshef, courtesy of the Mediated Matter Group. Color images available online at [www.liebertpub.com/3dp](http://www.liebertpub.com/3dp)

### Approach

Functional templating<sup>8</sup> of microbial activity through 3D printing of heterogeneous material distributions, or the ability to design a top-down material system that can inform bottom-up biological processes (such as guiding microbial growth for the purpose of photosynthesis), is a fundamental concept for the design of biologically augmented wearables. Our approach for designing *Mushtari* focuses on methods by which heterogeneous multimaterial 3D printing for the design of custom intermediate materials, in combination with novel additive manufacturing strategies, can be used for the fabrication of complex fluidic channels that create an artificial habitat for microbial growth.

### Organization

The article is organized in three sections: (1) Growing *Mushtari*, (2) Printing *Mushtari*, and (3) Augmenting *Mushtari*. In the first section, we show how complex channel geometries were generated and how heterogeneous material distributions within these channels were modeled. In the second section, we present a digital fabrication method for controlling material distribution using multimaterial 3D printing, using a novel liquid support material, which enables the fabrication of a vast interconnected network of internal channels. Finally—in the third section—we demonstrate the biocompatibility of the 3D printed materials in the context of microbial growth studies. The aforementioned three sections relate to their respective knowledge domains—computational design, additive manufacturing, and synthetic biology—that coalesce to a first-of-its-kind implementation of synthetic biology in the domain of 3D printing, and vice versa.

### Growing Mushtari

The design motivation behind *Mushtari* was to create a full-scale wearable with fluidic channels circumnavigating the human body in a dense, space-filling manner. To achieve this, the design involved a computational process that emulates natural growth in a controlled manner. This, in turn, led to the development of natural and organic-like structures, culminating in a design “symbiosis” between artificial (computational) growth of the *containing* environment and the natural (biological) growth of the *contained* microorganisms. As such, *Mushtari* was designed using a generative growth algorithm, which emulates biological growth by developing complex geometries over multiple iterations. Similar processes include, for example, Lindenmayer-Systems<sup>9</sup> (L-Systems), which are a widely used formal grammar, where rules are applied in parallel to generate branching structures. Reaction-diffusion equations provide another example, where partial differential equations are implemented for modeling the distribution of components within a reaction, mimicking phenomena of pattern formations that are characterized by variation of properties using multiple species (e.g., materials).<sup>10</sup> More recently, the usage of a simplified mass-spring system over a mesh with a selective refinement strategy has been proposed for the generation of cellular forms.<sup>11</sup>

Implementing a similar system, our approach allows us to inform the global or overall geometry, the local mesh geometry, as well as variations in material property distribution across length scales, by altering the relative strength of relaxation, attraction, and repulsion over several iterations as described below. This approach enabled the design of a *single* channel that “grows” over numerous iterations to generate a wearable with 58 meters of hollow internal structure. The channel uses variations in diameter—from 1 to 25 mm—as shown in Figure 2, as well as variations in transparency; locally graded within the wearable to create areas where photosynthetic microbes could receive light, thrive, and grow.

### General framework

The general framework driving the generation of *Mushtari* is shown in Figure 3. A geometric input representation (e.g., a triangle mesh, a set of line segments, or a point cloud) is first transformed into an intermediate representation. From this intermediate representation, a coarse implicit representation is generated. Information from these three representations is then used to deform the initial geometric representation. Finally, the deformed initial representation is topologically modified to react to the deformation of the object. This is done iteratively, such that a given input representation is continuously deformed and refined. As the process repeats, the deformations aggregate into the growth of a coherent form. For an exhaustive presentation showcasing 15 different derivations of this process, we refer to a study by Bader and Kolb.<sup>12</sup>

### Growth of polygonal lines

Figure 4a shows how the general framework can be adapted to animate the growth of a polygonal line that acts as a backbone for the fluid channel of the wearable. In this case, the input representation is a polygonal line, while the intermediate representation is a point cloud. The implicit representation

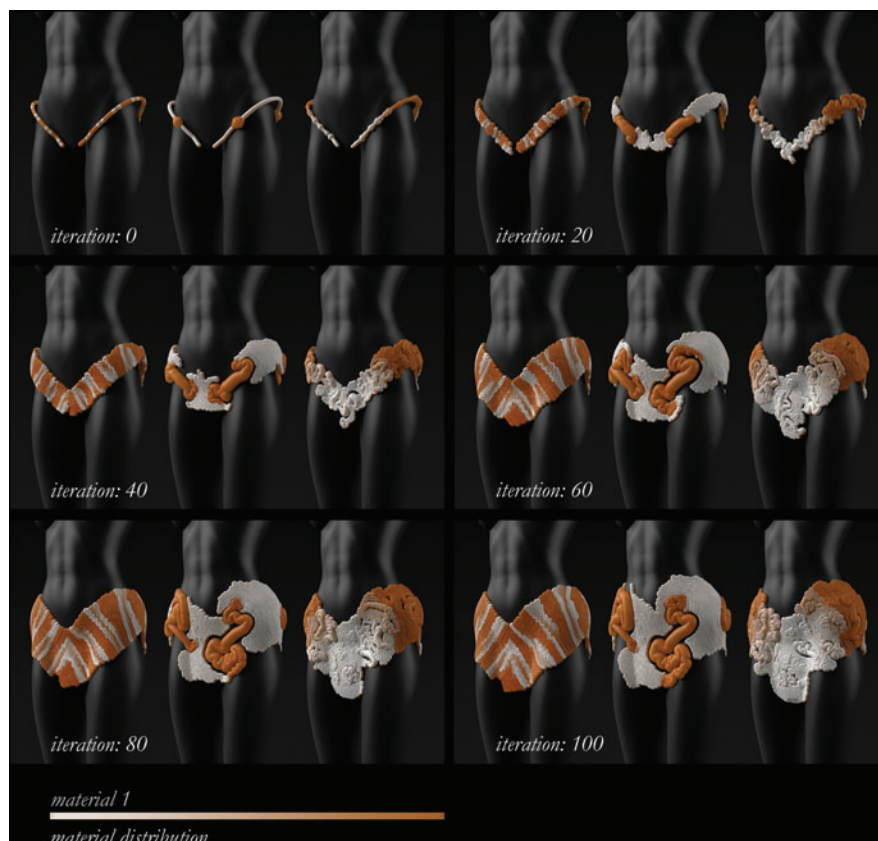


FIG. 2. Visualization of 100 iteration steps from three different growth variations used to generate the fluidic wearable, *Mushtari* (left, middle, and right orientations—in each panel). Shown are global- and local-scale controls over the generation of the fluidic channels, as well as the ability to tune material properties during computational growth. Materials shown in red represent transparent areas, while materials shown in white represent opaque areas. The left-most approach (in each panel) varies transparency as a periodic function of the length of the strand. The center approach varies transparency by the diameter of the tubing. In the right-most approach, material properties are assigned by regions. Color images available online at [www.liebertpub.com/3dp](http://www.liebertpub.com/3dp)

is a distance field,<sup>13</sup> given by the distances to the points of the intermediate representation and the associated radii. The deformation is described by a displacement of the vertices of the polygonal line. The subsequent topological transformation is performed by resampling of the line. The iterative nature of this process results in a continuous deformation of the input polygonal line.

We assume the polygonal line  $L$  is given by a set of vertices  $V_L = \{v_1, \dots, v_n\}$  and edges  $E_L = \{e_1, \dots, e_m\}, e_i \in V_L \times V_L$  where a position  $p_i = p_L(v_i)$  in  $\mathbb{R}^3$  is associated with each vertex  $v_i \in V_L$ . Then, the intermediate representation is given by a point cloud  $P = \{w_1, \dots, w_n\}$ , containing  $n$  points, one for each vertex of  $L$ , with positions  $p_P(w_i)$  offset along the edges of  $L$  and associated radii  $r(w_i)$ . From this, the

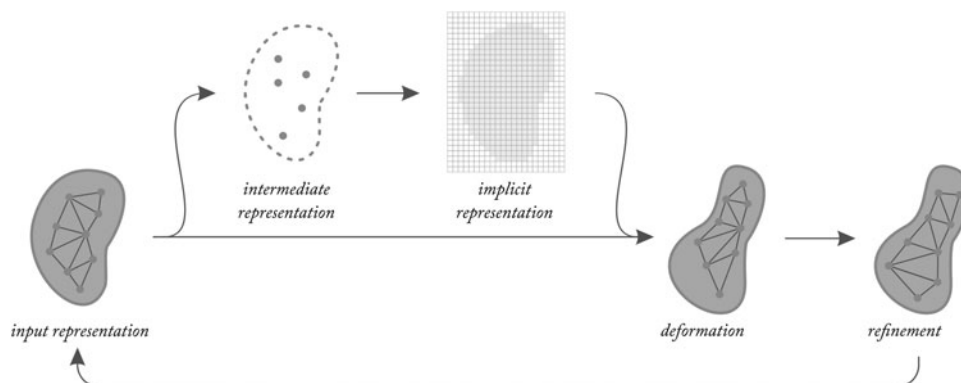


FIG. 3. Schematic overview of the general framework used for the generation of computationally grown structures.

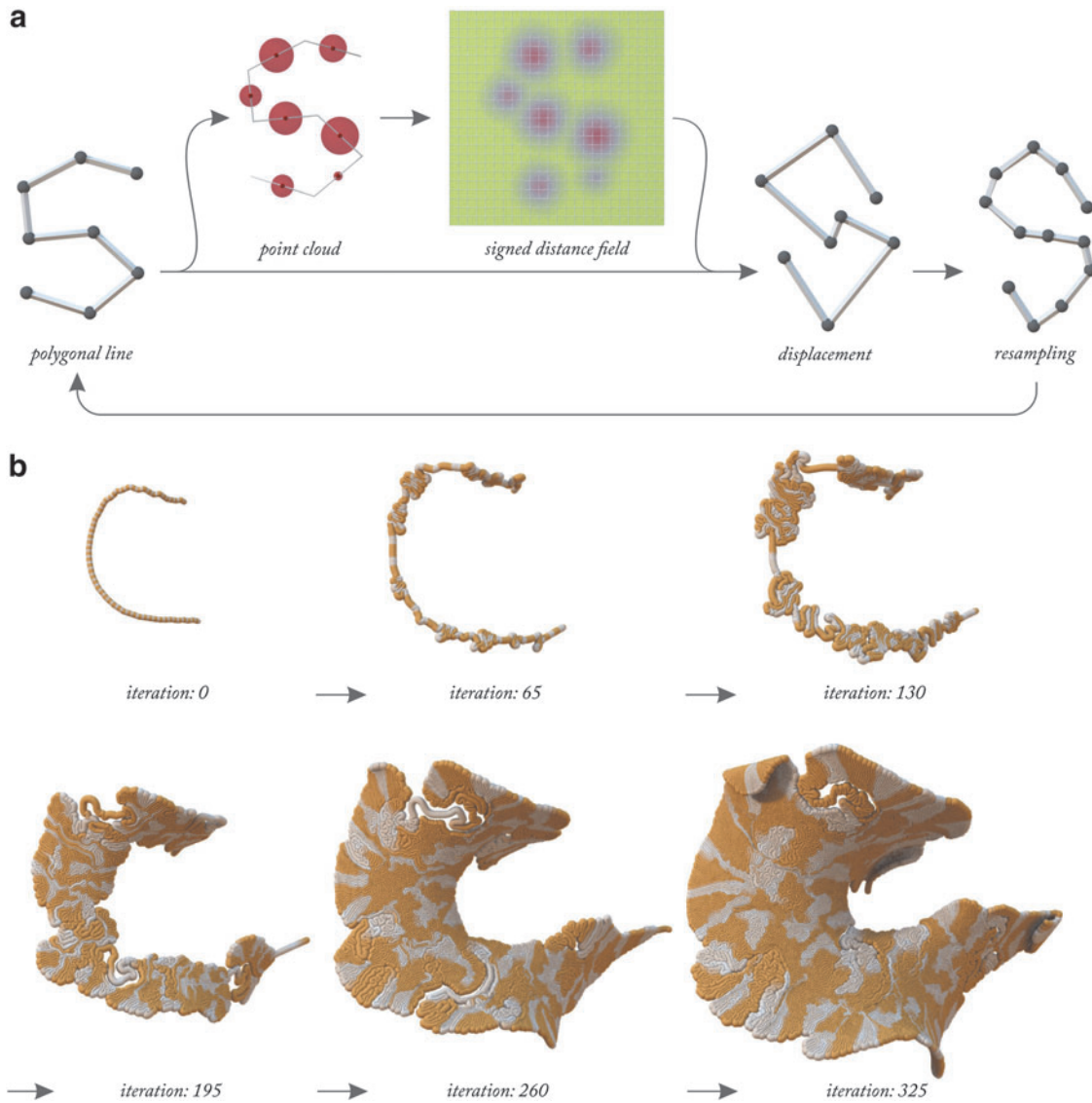


FIG. 4. **(a)** Example of the general framework applied to a *polygonal line*. **(b)** Several iterations of this process ultimately resulting in a compact coiled architecture. In this figure, the process is constrained to the tangent space of an underlying guiding triangular mesh (not shown). Color images available online at [www.liebertpub.com/3dp](http://www.liebertpub.com/3dp)

implicit representation is given again by a distance field  $d_P : \mathbb{R}^3 \rightarrow \mathbb{R}$  such that  $d_P(x) = \inf_{y \in \partial B} \|x - y\|$  where  $\partial B$  is the boundary of

$$B = \bigcup_{i=1}^n \{y \in \mathbb{R}^3 \mid \|p_P(w_i) - y\| \leq r(w_i)\}$$

In each iteration, the deformation from the input polygonal line  $L_j$  to the deformed line  $L_{j+1}$  is described by the displacement function  $\delta$ , which associates with each vertex  $v_i$  a displacement vector  $\delta_i = \delta(v_i)$  such that  $L_{j+1} = \{p_i + \Delta t \delta_i \mid v_i \in V_{L_j}\}$  and

$$\delta_i = -a \Delta d_P(p_i) \nabla d_P(p_i)$$

where  $a$  is a free parameter,  $\Delta d_P$  is the Laplacian, and  $\nabla d_P$  is the gradient of  $d_P$ . After the displacement, the polygonal line

is resampled such that all edges have the same length. An example of this process is shown in Figure 4b. For the final 3D printable geometry, we extracted a surface representation by volumetric expansion from the 1-dimensional strand, where the strand's local proximity to nearby points guides the enlargements of the 3D geometry.

#### Functional templating

The core motivation associated with biological augmentation of the device was to contain a sustainable coculture of photosynthetic microbes capturing solar energy and nourishing other heterotrophic microbial communities. The design required and involved *functional templating*,<sup>8</sup> achieved through high-resolution tunability of material properties, such as opacity. Transparent or translucent channels would enable the phototrophs' exposure to sunlight and the subsequent transfer of chemical energy in the form of fixed carbon

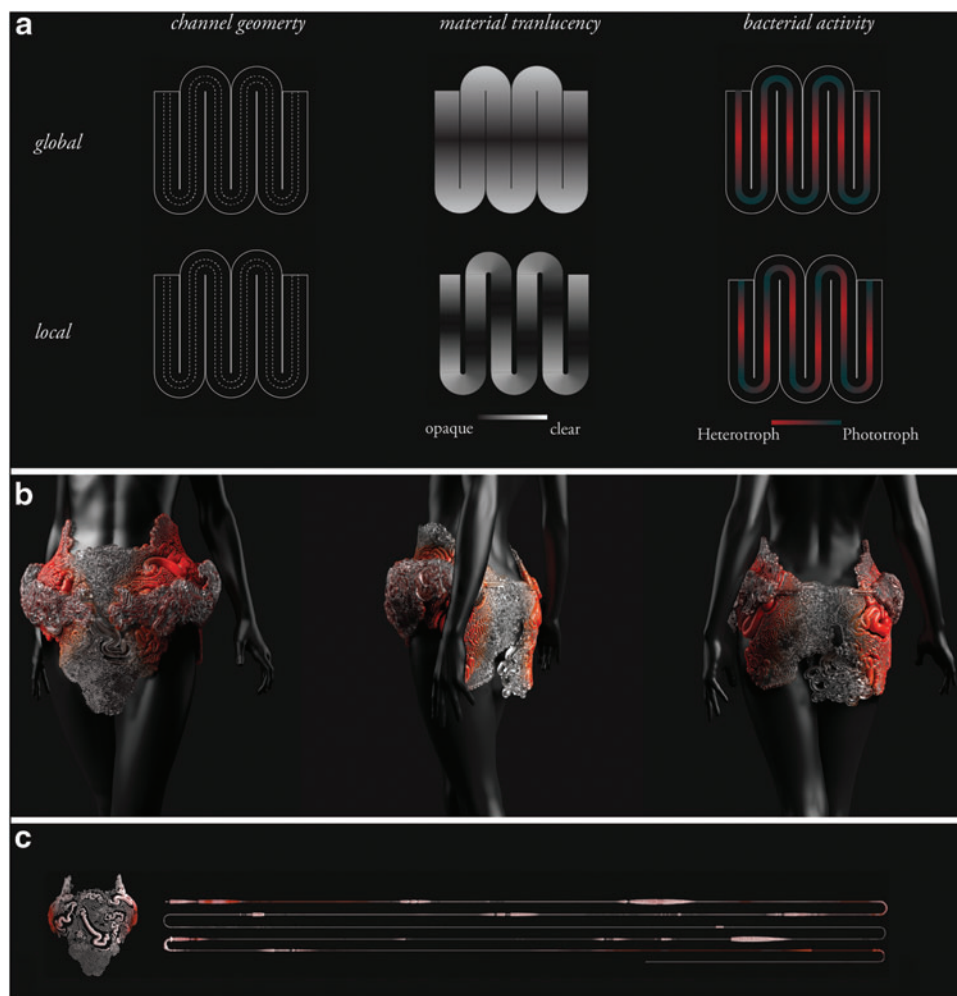


FIG. 5. (a) The desired effect of material transparency on microbial activity. In translucent regions, the coculture receives light, increasing phototrophic activity (*right column*). In opaque regions, the coculture is dark and the heterotrophs would consume the photosynthates, thus increasing their metabolic activity. Transparency can be controlled globally, as shown in the *upper middle column*, independently of the strand, or locally, shown in the *lower middle column*, using path-length parameterization as a guide for material distributions. (b) Implementation of the global heterogeneous modeling approach on the wearable. (c) Visualization of the unfolded strand showing how the overall (“global”) source-based approach influences local changes in opacity along the strand Figure 6. Color images available online at [www.liebertpub.com/3dp](http://www.liebertpub.com/3dp)

to heterotrophic bacteria such as *B. subtilis* and *E. coli*. Our design approach therefore necessitated the *parameterization of material properties for functional templating*. This approach is presented in Figure 5.

To enable functional templating via continuous control over transparent and opaque regions, we used heterogeneous material modeling techniques.<sup>14</sup> Material properties were either specified as a function of the path length of the grown strand, or globally defined by specifying external sources.<sup>15</sup> While the parameterized approach allows better control over local variation, the global approach yields better control of overall material distribution (the latter was chosen for *Mushtari*, as shown in Figure 5b). Figure 5c shows the generated fluid channel in its unfolded state, illustrating local material distributions required to achieve the global distribution in the final folded form. Modeled material distributions were subsequently fabricated using a Objet 500 Connex 3 multimaterial 3D printer (Stratasys Ltd.) by using the transparent VeroClear (RGD810) and rigid, opaque VeroRed materials.<sup>16</sup>

### Printing Mushtari

#### 3D printing a materially heterogeneous tract

To effectively template the containment and activity of fluid media within the wearable, it is necessary to digitally fabricate channels that are geometrically complex as well as materially and optically heterogeneous. The production of an optically heterogeneous single conduit poses significant technical challenges from an additive manufacturing perspective. Specifically, to fabricate a single channel with variable properties, the use of multipart assemblies with predefined and consistent properties, or—similarly—the use of tube inserts post-fabrication was deemed impractical. As such, to fabricate a continuous tract that is at once materially heterogeneous and hollow, we used a bitmap-printing approach to create controllable opacity gradients and leveraged a novel liquid support material strategy enabling the fabrication of vast channel networks.

### Multimaterial voxel printing of fluidic channels

To 3D print materially heterogeneous channels, we implemented a voxel-based 3D printing technique,<sup>17</sup> which enabled the digital fabrication of material property gradients. Modern multimaterial 3D printers<sup>18</sup> utilize an ink jet-like printing approach to construct parts by depositing UV-curable droplets of photopolymer resin in a layer-by-layer manner. By depositing distinct material droplets of base resins in high resolution (600 dpi in  $x$  and 300 dpi in  $y$ ), nearby material droplets will diffuse at a micron level, resulting in the formation of hybrid materials with intermediate properties. Controlling this high-resolution placement enables the creation of functionally graded materials at a fine scale. To achieve this level of control,

we implemented a custom 3D slicing and material distribution method,<sup>19</sup> which allows for the utilization of external data sources to evaluate heterogeneous material modeling methods *during* slicing, and, as such, enables for the computation of material distributions in high spatial resolution. These material modeling descriptions are used to generate binary 3D voxel matrices containing spatial droplet deposition descriptions for the 3D printer. Given that the 3D printer used in this study can print three different materials simultaneously (or four—including the support material), it is possible to generate three to four 3D matrices at the native resolution of the printer. These material deposition descriptions can be used to achieve highly precise functionally graded materials (Fig. 6). In this study, ratios of locally proximal deposited material droplets dictate the

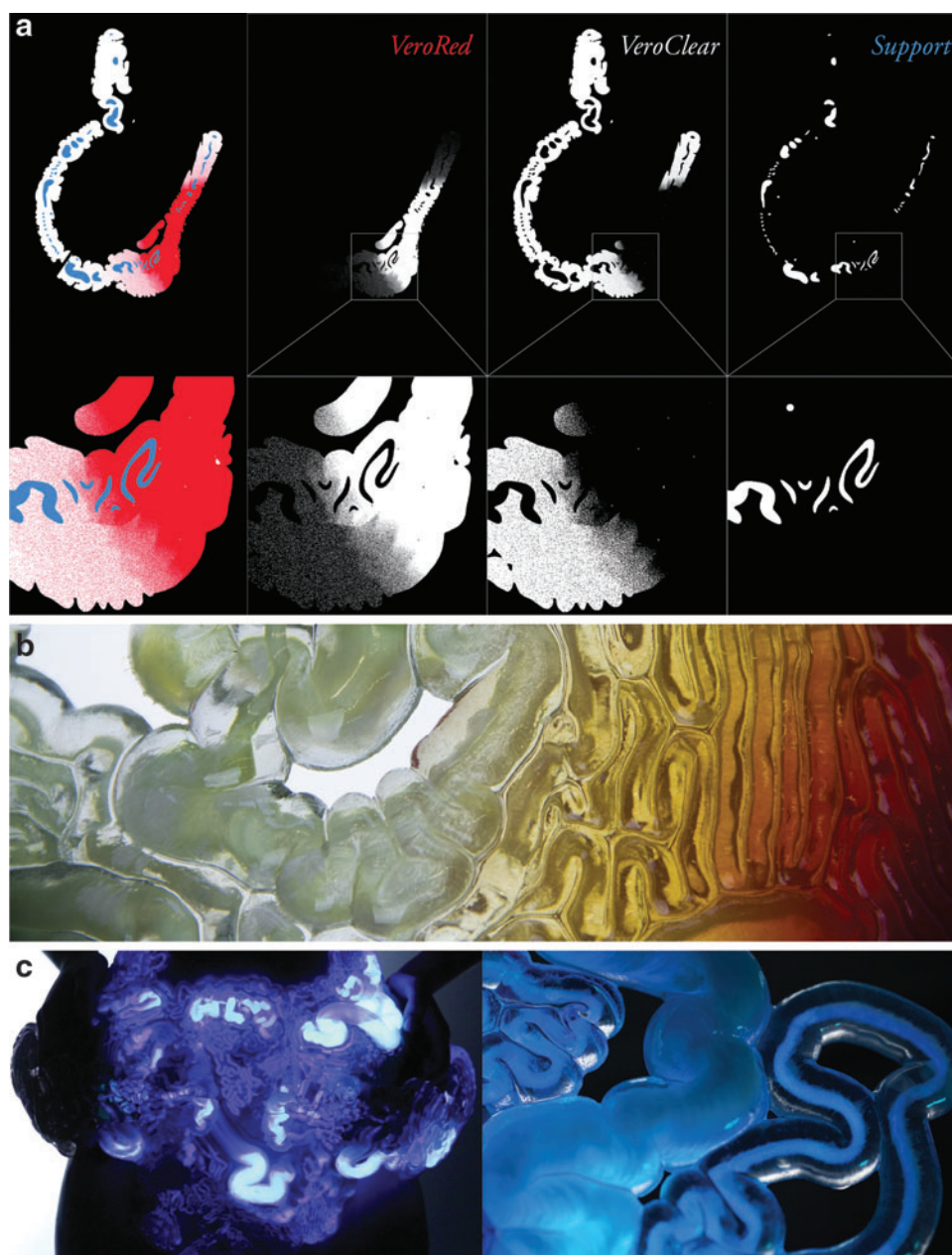


FIG. 6. (a) A single layer of the 3D material deposition description (*top*) highlighting areas where optical gradients are modeled (*bottom*). (b) Actual fabricated optical gradients with filled internal channels. (c) Hollow channels filled with chemiluminescent liquid for the purpose of visualization. Color images available online at [www.liebertpub.com/3dp](http://www.liebertpub.com/3dp)

functional properties of the printed material composites. As shown in Figure 6a, by continuously varying the ratio of opaque (VeroRed) to transparent (VeroClear) material droplets, we can achieve high control over opacity gradients in the 3D printed part, as shown in Figure 6b, which effectively allows us to implement desired functional templating.

In addition, this approach allows us to make use of high-resolution, highly precise Boolean operations without modifying the actual geometry. We achieve this by specifying to use support material over model materials in areas that are desired to be hollow in the final form. This allows us to create physically hollow channels, after the cleaning process, on arbitrary complex geometries without modifying the actual shape description as shown in Figure 6c.

While the VeroClear materials are intrinsically transparent, the deposition of support material during the printing process results in a partial roughening of the VeroClear following support material removal, with the resulting part exhibiting partially diminished optical clarity. While this small reduction in optical clarity was adequate for our specific application, increased optical clarity can be achieved by polishing and/or lacquering the 3D printed part to reduce this intrinsic surface roughness.

While the build volume of the 3D printer used in this study measures  $50 \times 40 \times 20$  cm, to achieve a wearable-scale object, we split the form into a five-piece assembly such that each piece could fit in the build volume of the printer. Each piece featured a single long channel and the combined five channels stretched 58 meters in total with diameters ranging from 1 to 25 mm.

#### *Printing a hollow channel*

Multimaterial 3D printers<sup>18</sup> utilize a separate support material to enable the printing of complex geometries with overhangs or internal structures. During the printing process, this gel-like support material (SUP705) is added to any internal structure, including the fluidic channel network. Once the printing process is complete, the gel-like support material is abrasively removed using a high-pressure water jet that must come in direct contact with the support material. This process works well for large bulky geometries or those with short internal voids, but is not suitable for long fluidic channels due to the restricted channel access. To overcome this barrier, we investigated the use of two alternative support methods; an available soluble support (SUP707) and an experimentally developed liquid support. The soluble support material is a polymer material that dissolves in water and can be substituted for the typical gel support in the normal 3D printing workflow. The liquid support method uses a material with similar prepolymer material properties but cannot be polymerized by UV light. This liquid support can be printed into internal channels by assigning an STL mesh or a separate 3D voxel matrix of the inner channel geometry to the liquid support material.

#### *Characterization and evaluation of support methods*

Soluble support and liquid support present two potential options for creating internal fluidic channels within the wearable. To evaluate the two support methods, we designed test pieces that contained channels of 1 to 20 mm in diameter, as shown in Figure 7 (rightmost column). We printed the test piece using normal support (SUP 705), soluble support

(SUP707), and liquid support. Cross sections of test pieces were examined using optical microscopy. Images were acquired using a Vividia 2.0 MP handheld USB Digital Endoscope, as shown in Figure 7. The test pieces printed using liquid support in a horizontal orientation were the only test pieces that could be entirely cleared of support and liquid could easily pass through all channels (A–G) for each of the three sample replicates. In test pieces printed using soluble and liquid support in a vertical orientation, channels greater or equal to 1 mm in diameter (B–G) could be cleared. In test pieces printed with the traditional gel support, only channels greater than or equal to 3 mm (E–G) could be cleared. Three replicates were measured for each support type and three technical replicates were performed for each measurement. Table 1 summarizes the expected and measured dimensions of the test piece cross sections.

To test the suitability of each support material for the complex internal fluidic channels of the wearable, we designed a second test piece as shown in Figure 8 to reflect the geometry of the final wearable. The test piece featured five inlets and a channel diameter that ranged from 1.5 to 12 mm. First, the piece was printed with soluble support, which was unable to be cleared from the piece even after multiple attempts. We then printed the same patch using liquid support, which was cleared successfully, and demonstrated that liquid could easily flow through this piece from the inlet to the outlet. Even though the second test piece featured larger minimum diameter channels compared with the first test piece and contained multiple inlets, the soluble support still could not be cleared from the second test piece. This finding suggests that the irregular geometry, including multiple branches, variable diameters, and small radii of curvature, factored into our inability to clear soluble support from the channels. Based on these two test pieces, we used the liquid support material for printing the wearable.

In summary, we found that both the soluble and liquid support materials can be used to fabricate fluidic channels using multimaterial 3D printing. Liquid support can be successfully used to print channels with diameters as small as 300 microns but results in additional channel surface roughness. Soluble support has higher print quality, is more accurate, and creates less surface roughness than liquid support, but the soluble support could not be cleared from the smallest channels in the test pieces.

#### *Visualizing Mushtari's inner channels*

The final piece was printed with many 1.5 mm diameter inlets throughout the fluidic network, which were used for removing any remaining liquid support material and for filling the piece with test liquid. We visualized the channels by filling *Mushtari* (Fig. 6b). In addition to the clear media used for initial testing, *Mushtari* was also filled with a chemiluminescent liquid (Fig. 6c) to better visualize the internal channel network.

A 22-gauge needle was press fit into the inlets, and after filling the piece, the inlets were capped with small plugs that were 3D printed from the same materials as the wearable to create a watertight seal.

While preliminary tests revealed that all channels in the five pieces were cleared of liquid support, we found that we were unable to manually flow liquid from inlet to outlet in the

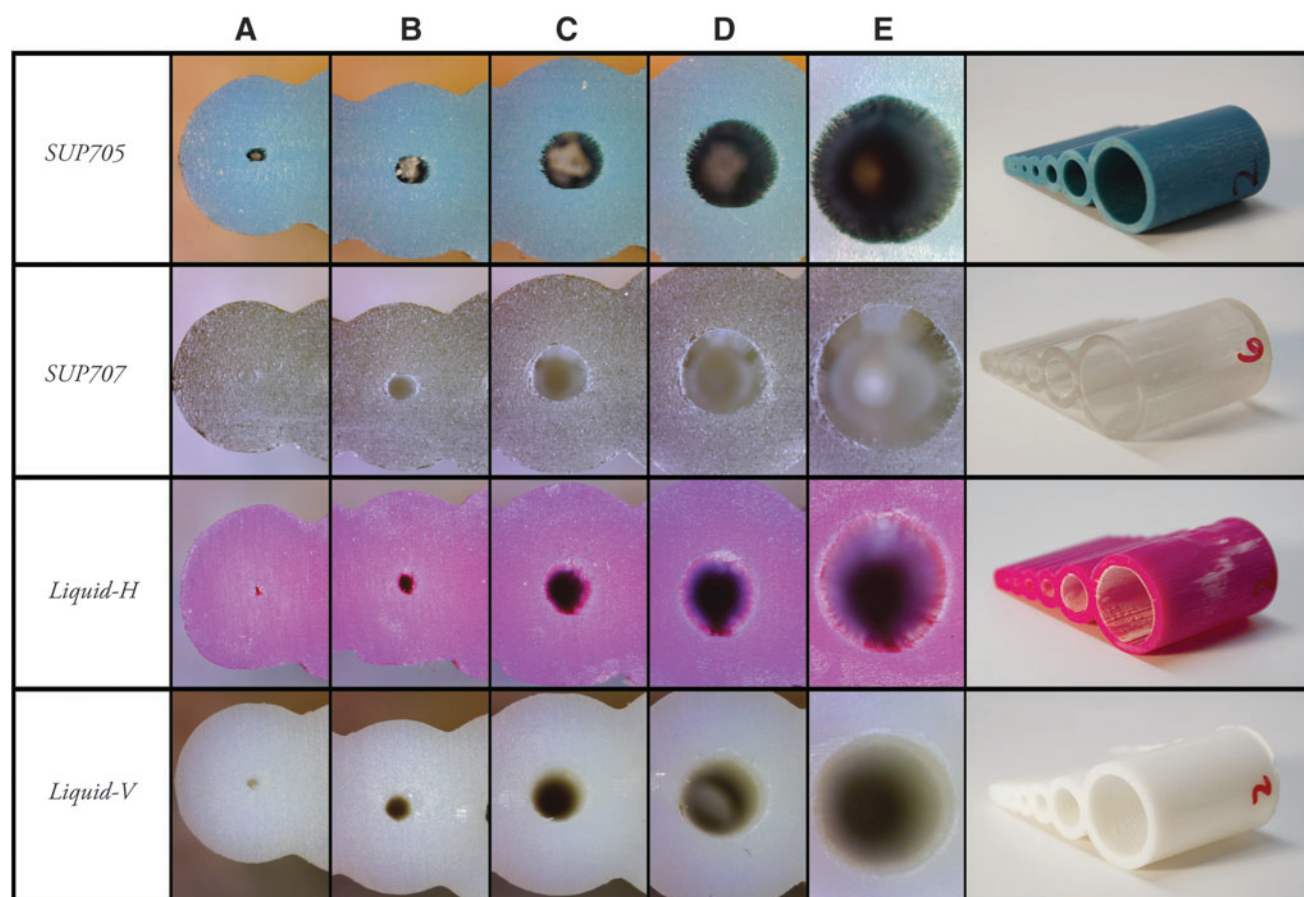


FIG. 7. Representative optical images of test piece cross sections that were printed using the three support material methods. Color images available online at [www.liebertpub.com/3dp](http://www.liebertpub.com/3dp)

complete fluidic network. While in one piece, we were able to flow the injected liquid 3.5 meters through a channel section with diameters that ranged from 1.4 to 11 mm, and as the path length increased, the pressure required for complete channel filling became insurmountable, likely due to accumulated resistance from variable channel diameter, channel length, and channel curvature. Information regarding these parameters is critical for future geometries that may be designed to culture bacterial communities for extended time periods, and which may be structurally optimized by fluid flow simulations during the initial design process. Under such culture

conditions, flow will be important for the exchange of nutrients and channel diameter may be influenced by the growth of biofilms on the channel walls based on their diameter and curvature.<sup>20</sup>

#### Augmenting Mushtari

Synthetic biology is an interdisciplinary field that applies an engineering approach to biology.<sup>21</sup> As such, it alludes to practices that enable the engineering of molecules, cells, and microorganisms to perform specific tasks.<sup>21</sup> In this vein,

TABLE 1. MEAN AND STANDARD DEVIATION OF DIAMETERS A–G (MM) OF THE TEST PIECES WITH VARIOUS SUPPORT MATERIALS

Diameter	Expected value	Normal	Soluble	Liquid-H	Liquid-V
A	0.5	0.46 ± 0.03	0.41 ± 0.03	0.3 ± 0.04	0.36 ± 0.04
B	1	0.97 ± 0.03	0.88 ± 0.05	0.73 ± 0.06	0.90 ± 0.05
C	2	2.02 ± 0.05	1.96 ± 0.05	1.76 ± 0.05	1.92 ± 0.06
D	3	3.10 ± 0.07	2.96 ± 0.08	2.82 ± 0.07	3.0 ± 0.1
E	5	5.2 ± 0.1	5.0 ± 0.1	4.9 ± 0.1	5.0 ± 0.1
F	10	10.0 ± 0.2	9.9 ± 0.2	9.8 ± 0.3	9.8 ± 0.2
G	20	20.0 ± 0.3	19.9 ± 0.3	19.0 ± 0.3	19.8 ± 0.3

The mean and standard deviation of each diameter per support type were calculated using three replicates printed and measured for each support type. Diameters were measured in the direction of the print orientation. Normal, soluble, and Liquid-H were printed in the same horizontal orientation. Liquid-V was printed in a vertical orientation.

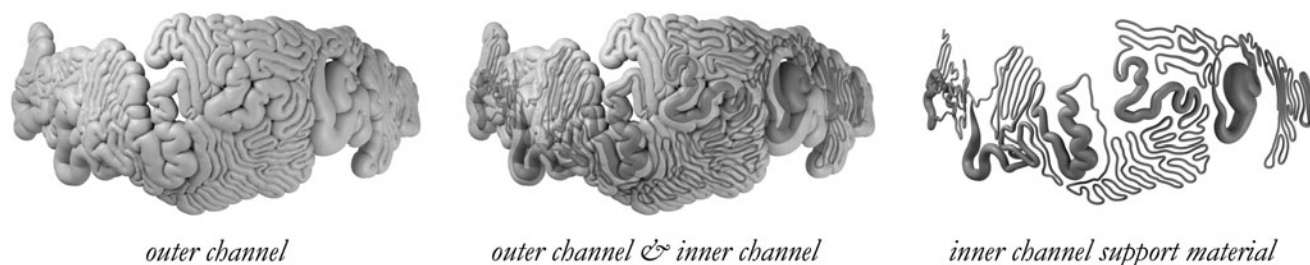


FIG. 8. Visualization of smaller scale test piece used. The image on the *left* shows the actual shape of the printed piece. The image in the *middle* and the image on the *right* visualize how the support material (*blue*) is distributed and printed inside the wearable to achieve a hollow channel.

*Mushtari* was designed to act as a potential “host” environment for the coculture of engineered microorganisms that make up a synthetic “community.” Synthetic biologists use disparate bacteria to capitalize on each microbe’s unique physiological specialties and evolved capabilities. *E. coli* is arguably the best-studied model bacterium<sup>22</sup> and has been modified to produce useful products, including scents,<sup>2</sup> colors,<sup>3</sup> and fuels.<sup>4</sup> However, *E. coli* is not best suited for all applications. For instance, *B. subtilis*, a popular gram-

positive model bacterium found in soil, can secrete large quantities of proteins, making it an appealing option for the production of commercial enzymes and protein-based biopharmaceuticals.<sup>23</sup>

Both *E. coli* and *B. subtilis* are heterotrophic, which means they must obtain their organic carbon from the external environment. In contrast, phototrophic microbes, including cyanobacteria and algae, can capture solar energy and use it to fix carbon dioxide. In nature, microbial communities are complex

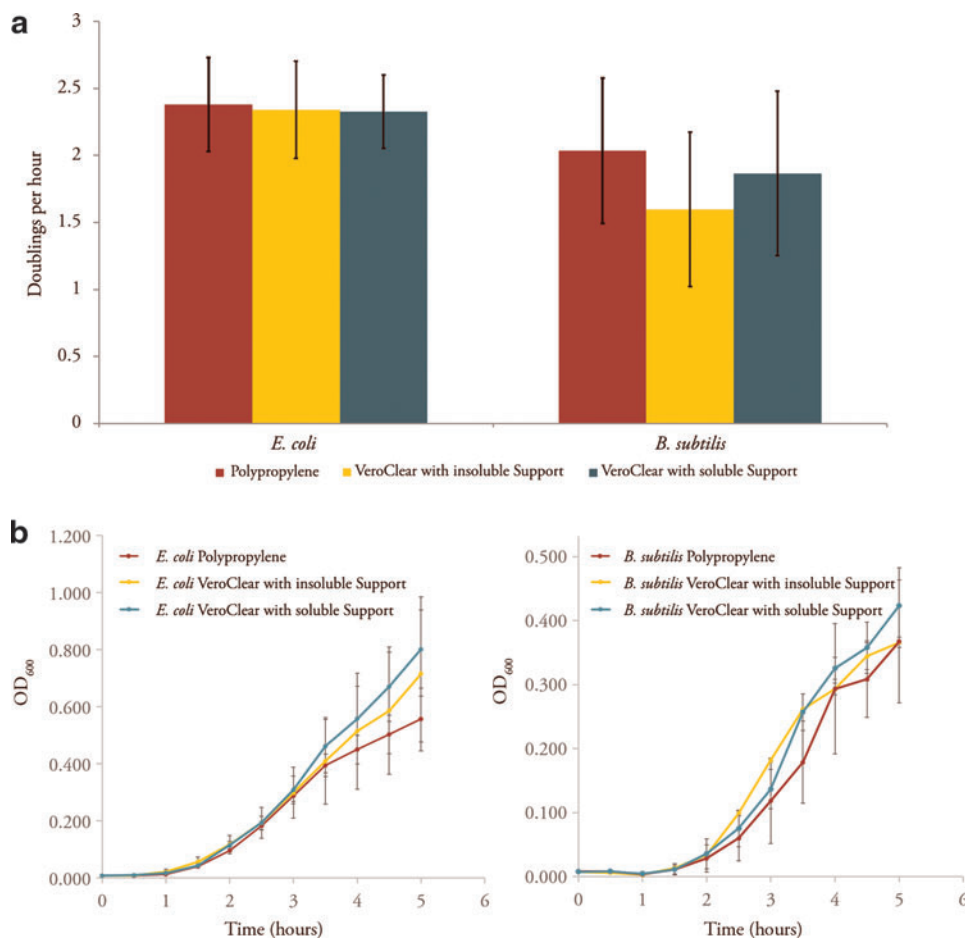


FIG. 9. **(a)** Comparison of growth rates (doublings per hour) of *Escherichia coli* and *Bacillus subtilis* in various tube materials. Error bars represent the standard deviation between at least six biological replicates. Representative growth of *E. coli* **(b, left)** and *B. subtilis* **(b, right)** in different tubes. Error bars represent the standard deviation among three biological replicates grown on the same day. Color images available online at [www.liebertpub.com/3dp](http://www.liebertpub.com/3dp)

mixtures of different species that capitalize on different metabolic capabilities, allowing for an efficient division of labor. Synthetic biologists have begun to take advantage of this organization by creating new systems that combine both phototrophic and heterotrophic assemblages.<sup>24</sup> *Mushtari* was engineered to provide an environment for such a consortium.

### Cytotoxicity studies

As one aim of the 3D printed wearable is to host microorganisms inside the hollow channels, the cytotoxicity of the 3D printed materials needed to be investigated. To investigate the potential cytotoxicity of the 3D printed pieces and their impact on microbial growth, specialized tubes were printed to mimic the plastic labware used in standard microbial culture. The tubes had similar geometry to a standard 14 mL polypropylene culture tube (Falcon; Corning), while the 3D printed culture tubes were designed to be thicker in an attempt to minimize potential fissures and leakage. Before the 3D printed pieces could be used to culture microbes, they were pretreated and sterilized. Pretreatment involved removing support materials with a water jet (PowerBlast High Pressure Water Cleaner; Balco) followed by submersion in 2% sodium hydroxide for 1 h. Another cleaning with the water jet followed. This process was then repeated, such that parts were exposed to the sodium hydroxide solution twice. The 3D printed parts were next boiled, rinsed in distilled water, and then autoclaved to achieve sterility. Sterility was checked via the addition of rich media to tubes after sterilization. After overnight incubation at 37°C, no bacterial growth was visible. While many of the 3D printed tubes could be successfully used for cell culture, others proved not to be watertight. As this was most frequently seen in sterilized pieces as opposed to untreated test pieces, future studies will focus on optimizing the treatment and sterilization protocols to decrease harshness and, consequently, limit leakage.

For the microbial growth studies, two model bacterial species, *E. coli* and *B. subtilis*, were used. *E. coli* (BW25113) and *B. subtilis* (168, ATCC #23857) were struck from frozen stocks onto Luria broth (LB) plates. Individual colonies were picked for biological replicates and grown in liquid LB. After growth either overnight or to a visually turbid state at 37°C, cultures were diluted to a low OD<sub>600</sub> (~0.05) as measured by cuvette in fresh liquid LB. These cultures were then split between three conditions: (1) polypropylene tubes as controls; (2) VeroClear tubes with insoluble support (SUP705) material; and (3) VeroClear tubes with soluble support (SUP707) material (Fig. 9a). Each uncapped culture tube was placed inside a 50 mL polypropylene tube (Falcon; Corning), which was then capped. To prepare the negative controls, 5 mL of LB media were added to three VeroClear tubes, printed with either insoluble or soluble support material, and three polypropylene tubes. These tubes were also placed inside 50 mL BD Falcon polypropylene tubes. All tubes were cultured in a 37°C incubator shaking at 200 rpm. Measurements were taken every 30 min until the cells appeared to hit stationary growth. OD<sub>600</sub> measurements were taken using a 96-well plate reader. Media blank readings were subtracted and these values are reported directly in the representative data shown in Figure 9b,c. To calculate the doubling time, the log base two of each sample was calculated. The time series for each rep-

licate was plotted with log<sub>2</sub> (OD<sub>600</sub> value) versus hours. For each condition, a line of best fit was determined for over each 1.5-h period. The maximum growth rate with an R<sup>2</sup> value higher than or equal to 0.96 is reported. To quantify the variation between the biological samples for each condition, we then measured the doublings per hour for each biological sample and calculated the standard deviation. We found no statistically significant difference in the growth rates of *E. coli* or *B. subtilis* in the 3D printed tubes (with either support condition) in comparison to the standard control Falcon tubes. These results demonstrate that the microbial model organisms *E. coli* and *B. subtilis* can be grown within the 3D printed vessels with no measurable negative growth effects. Future work will explore the biocompatibility of these materials for the culture of other engineered heterotrophic and autotrophic microbes to add functionality to the consortia in complex fluidic systems.

### Conclusions and Future Work

The fields of Synthetic Biology and 3D Printing are developing rapidly, yet independently of each other. *Mushtari*—the wearable and its associated suite of tools, techniques, and technologies—demonstrates and points toward design possibilities that lie at the intersection of these fields as well as the relevance of such intersection to applications in product design. We designed a fluidic wearable with the ultimate goal of mediating the functionality of microbial communities by “templating” their containing environments using multimaterial 3D printing. As such, the experimental research presented herein, showcases a first of its kind fluidic wearable demonstrating *computational growth of 3D printable multimaterial fluidic channels at product scale*.

The project accomplished three goals, relevant to three research domains, namely: computational design, additive manufacturing, and synthetic biology. Those include the following: (1) development and implementation of a computational approach for generating product-scale fluidics and heterogeneous modeling of material properties for functional templating; (2) implementation, characterization, and evaluation of support material formulations for creating fluidics at product scale; and (3) cytotoxicity evaluations of photopolymeric 3D printed materials with model microbial species.

The current design of *Mushtari* embodies exciting research challenges that lie at the intersection of additive manufacturing and synthetic biology. Those include (1) challenges associated with charging the wearable, that is, charging required media (cells or tissues) in and out of the product; (2) challenges associated with keeping cells and cultures healthy and alive (e.g., sterility, gas exchange, and biocompatibility for other microbial species); and (3) challenges associated with extracting any “product” (e.g., sugar, fragrance, or biofuel) that has been generated by the microbes contained within the wearable.

In this article, we demonstrated that by using currently available multimaterial 3D printers, it is possible to control the deposition of multiple materials at the printer’s native resolution. In the context of *Mushtari*, we focused on the control of material opacity and fluid containment. Integrating flexible materials into the design process would enable us to also control the elastic modulus, which, in turn, could open up

many new design possibilities. Such opportunities may include wearable skins that not only *contain* biological media but can also *filter* such media in a selective manner. Given that modern multimaterial 3D printers<sup>18</sup> can print in ca. 32  $\mu\text{m}$  voxel resolution, we point out the possibility that increasing the resolution of 3D printing systems would allow for the creation of selectively permeable membranes and pores. This could enable the production of a more sophisticated and regulated transport and filtration system inside the wearable, which exchanges and interacts with the wearer. In addition, therapeutic compounds created within the fluidic system could be stored in specific areas and locally administered to the skin. Finally, by combining advanced computational design strategies for digital growth with multimaterial 3D printing in high spatial resolution as shown herein, *Mushtari* paves the way toward multifunctional objects with spatiotemporal property variation in high resolution. Single material systems such as *Mushtari* will, in the future, enable the design and production of “breathing” and “living” wearables that can interact with our bodies and our environment, forming a true material ecology across scales.

### Acknowledgments

The authors thank Naomi Kaempfer, Director of Art, Fashion and Design at Stratasys, and related team members—Tal Ely and Yoav Bressler—for their insight and dedication in producing *Mushtari*. The company’s support has enabled the use of the Objet500 Connex3 multimaterial 3D printer. The authors acknowledge David Kong and Lincoln Lab (Sponsor Award ID is 7000345090) for recent insights inspired by *Mushtari*—its design and production. The authors also acknowledge Yoram Reshef for his photographs of the final design, as well as Paula Aguilera and Jonathan Williams for their support on additional visual materials. This research was supported, in part, by the National Science Foundation Award DGE1144152, Department of Energy DE-SC0012658 “Systems Biology of Autotrophic-Heterotrophic Symbionts for Bioenergy,” SynBERC, and the Wyss Institute for Biologically Inspired Engineering.

### Author Disclosure Statement

No competing financial interests exist.

### References

- Hays SG, Patrick WG, Ziesack M, Oxman N, Silver PA. Better together: engineering and application of microbial symbioses. *Curr Opin Biotechnol* 2015;36:40–49.
- Thanasomboon R, Waraho D, Cheevadhanarak S, Meechai A. Construction of Synthetic *Escherichia coli* reducing s-linalool. *Proceedings of the 3rd International Conference on Computational Systems-Biology and Bioinformatics* 2012;11:88–95.
- August PR, Grossman TH, Minor C, Draper MP, MacNeil IA, Pemberton JM, *et al.* Sequence analysis and functional characterization of the violacein biosynthetic pathway from *Chromobacterium violaceum*. *J Mol Microbiol Biotechnol* 2000;2:513–519.
- Lee SK, Chou H, Ham TS, Lee ST, Keasling JD. Metabolic engineering of microorganisms for biofuels production: From bugs to synthetic biology to fuels. *Curr Opin Biotechnol* 2008;19:556–563.
- Nervous System. Kinematics Dress—Nervous System. Available at <http://n-e-r-v-o-u-s.com/projects/sets/kinematics-dress/> (accessed May 06, 2016).
- Ho CMB, Ng SH, Li KHH, Yoon YJ. 3D printed microfluidics for biological applications. *Lab Chip* 2015;15:3627–3637.
- Oxman N, Ortiz C, Gramazio F, *et al.* Material ecology. *Comput Aided Design* 2014;60:1–2.
- Oxman N. Templating Design for Biology and Biology for Design. *Archit Design* 2015;85:100–107.
- Prusinkiewicz P. Graphical applications of L-systems. in *Proceedings of graphics interface*, 1986.
- Turing AM. The chemical basis of morphogenesis. *Philos Trans R Soc Lond B Biol Sci* 1952;237:37–72.
- Lomas A. Cellular Forms: An Artistic Exploration of Morphogenesis. ACM SIGGRAPH 2014 Studio, 2014.
- Bader C, Kolb D. A unified approach to grown structures. Available at [www.youtube.com/watch?v=9HI8FerKr6Q](http://www.youtube.com/watch?v=9HI8FerKr6Q) (accessed May 6, 2016).
- Jones MW, Bærentzen JA, Šrámek M. 3D distance fields: A survey of techniques and applications. *IEEE Trans Vis Comput Graph* 2006;12:581–599.
- Kou XY, and Tan ST. Heterogeneous object modeling: A review. *Comput Aided Design* 2007;39:284–301.
- Tan ST, Siu YK. Source-based heterogeneous solid modeling. *Comput Aided Design* 2002;34:41–55.
- Stratasys, Ltd., Polyjet Materials: A range of possibilities. Stratasy, Ltd., Rehovot, Israel, 2014.
- Doubrovski EL, Tsai EY, Dikovskiy D, Geraedts JM, Herr H, Oxman N. Voxel-based fabrication through material property mapping: A design method for bitmap printing. *Comput Aided Design* 2015;60:3–13.
- Omer S. PolyJet Matrix™ Technology A New Direction in 3D Printing. Stratasy, Ltd., Rehovot, Israel, 2009.
- Bader C, Kolb D, Weaver JC, Oxman N. Data-driven material modeling with functional advection for 3D printing of materially heterogeneous objects. *3D Print Addit Manuf* 2016;3:71–78.
- Rusconi R, Leceuyer S, Guglielmini L, Stone HA. Laminar flow around corners triggers the formation of biofilm streamers. *J R Soc Interface* 2010;7:1293.
- Baldwin G, Bayer T, Dickinson R, Ellis T, Freemont PS, Kitney RI, *et al.* *Synthetic Biology—A Primer*. Imperial College Press, London, 2012.
- Cooper GM. *The Cell: A Molecular Approach*, 2nd edition. Sunderland (MA): Sinauer Associates, 2000.
- van Dijk JM, Maarten J, Hecker M. *Bacillus subtilis*: From soil bacterium to super-secreting cell factory. *Microb Cell Fact* 2013;12:1.
- Goers L, Fremont P, Plozzu KM. Co-culture systems and technologies: Taking synthetic biology to the next level. *J R Soc Interface* 2014;11:pii: 20140065.

Address correspondence to:

Neri Oxman  
MIT Media Laboratory  
School of Architecture and Planning  
Massachusetts Institute of Technology  
75 Amherst Street, E14-433C  
Cambridge, MA 02139

E-mail: neri@mit.edu